Mon. Not. R. Astron. Soc. **000**, 1–12 (2007) Printed 19 November 2008 (MN LATEX style file v2.2)

Hubble Space Telescope Survey of the Perseus Cluster: II. Photometric scaling relations in different environments

S. De Rijcke[1], S. J. Penny[2], C. J. Conselice[2], S. Valcke[1], E. V. Held[3]
[1] *Sterrenkundig Observatorium, Universiteit Gent, Krijgslaan 281, S9, B-9000, Gent, Belgium*
[2] *School of Physics & Astronomy, University of Nottingham, Nottingham NG7 2RD, UK*
[3] *Osservatorio Astronomico di Padova, INAF, vicolo dell'Osservatorio 5, 35122 Padova, Italy*

Accepted 1988 December 15. Received 1988 December 14; in original form 1988 October 11

ABSTRACT

We investigate the global photometric scaling relations traced by early-type galaxies in different environments, ranging from dwarf spheroidals, over dwarf elliptical galaxies, up to giant ellipticals ($-8\,\mathrm{mag} \gtrsim M_V \gtrsim -24$ mag). These results are based in part on our new HST/ACS F555W and F814W imagery of dwarf spheroidal galaxies in the Perseus Cluster. The full sample, built from our HST images and from data taken from the literature, comprises galaxies residing in the Local Group; the Perseus, Antlia, Virgo, and Fornax Clusters; and the NGC5898 and NGC5504 groups.

Photometric parameters, such as the half-light radius, the central surface brightness, and the Sérsic exponent n are used to parameterize the light distributions and sizes of early-type galaxies. These parameters all vary in a continuous fashion with galaxy luminosity over a range of more than six orders of magnitude in luminosity. We also find that all early-type galaxies follow a single color-magnitude relation, which we interpret as a luminosity-metallicity relation for old stellar populations. These scaling relations are almost independent of environment, with Local Group and cluster galaxies coinciding in the various diagrams. As an example, due the presence of a population of very low surface brightness dSphs in the Fornax cluster, which may be tidally heated dwarf galaxies, the Fornax dSph population is on average only 0.2 mag arcsec^{-2} fainter than the Local Group dSph populations. This offset is much too small to destroy the global relation between luminosity and central surface brightness.

We show that at $M_V \sim -14\,\mathrm{mag}$, the slopes of the photometric scaling relations involving the Sérsic parameters change significantly. This contradicts previous claims that the relations involving Sérsic parameters are pure power-laws for all early-type galaxies and are, therefore, more fundamental than other photometric scaling relations derived from them. We argue that these changes in slope reflect the different physical processes that dominate the evolution of early-type galaxies in different mass regimes. As such, these scaling relations contain a wealth of information that can be used to test models for the formation of early-type galaxies.

Key words: galaxies: dwarf – galaxies: fundamental parameters – galaxies: structure – galaxies: clusters: general

1 INTRODUCTION

Dwarf spheroidal galaxies (dSphs) are faint stellar systems ($M_V \gtrsim -14$ mag) with smooth elliptical isophotes. They are presumed to be the faint analogs of dwarf elliptical galaxies (dEs), which are usually defined as lying in the luminosity range $-19\,\mathrm{mag} \lesssim M_V \lesssim -14$ mag. Being found typically not more than a few hundred kiloparsecs away from a massive galaxy or in groups and clusters of galaxies, they show a strong predilection for high-density environments (Mateo 1998; Grebel, Gallagher, Harbeck 2003). Their dynamical mass-to-light ratios, derived by fitting dynamical models to their stellar velocity dispersion profiles or based on stability arguments, vary from a few tens up to a few hundreds, in solar units (Mateo 1998; Łokas 2002; Kleyna et al. 2005; De Rijcke et al. 2006; Lewis et al. 2007; Mateo, Olszewski, Walker 2008; Penny et al. 2008). This high mass-to-light ratio suggests the presence of copious amounts of dark matter that

help protect the embedded stellar body of the dSph against the tidal forces of the massive host galaxy or of the galaxy cluster or group in which the dSph resides. This would explain why only a handful of dSphs in the Local Group show clear signs of an ongoing interaction despite being close satellites of either the Milky Way or M31 (Johnston, Spergel, Hernquist 1995; Mateo et al. 1996; McConnachie & Irwin 2006; Ségall et al. 2007; Lewis et al. 2007). Many dSphs and dEs still contain an interstellar medium and some even host low-level star formation (Blitz & Robishaw 2000; Grebel, Gallagher, Harbeck 2003; Conselice et al. 2003; De Rijcke et al. 2003; Buyle et al. 2005; Lisker et al. 2006; Young et al. 2007), showing that supernova explosions are not very efficient at expelling gas (Marcolini, Brighenti, D'Ercole 2003; Valcke, De Rijcke, Dejonghe 2008).

Bright elliptical galaxies, or Es, and dEs follow the same photometric and kinematic scaling relations (Graham & Guzmán 2003; Matković & Guzmán 2005; De Rijcke et al. 2005; Smith Castelli et al. 2008). In the luminosity interval -24 mag $\lesssim$ M_V $\lesssim$ -14 mag the parameters of the Sérsic profile follow simple power-laws as a function of luminosity and early and late type galaxies trace parallel Tully-Fisher relations (De Rijcke et al. 2007). From this wealth of data a picture of (dwarf) galaxy formation emerges that suggests an underlying unity in the physics driving the formation and evolution of stellar systems, with the environment playing a role that is in many situations subordinate to that of internal processes. More specifically, numerical simulations and semi-analytic models of galaxy formation within a ΛCDM cosmology can account for the observed scaling relations when taking into account supernova feedback in galactic gravitational potential wells steepening with galaxy mass (Carraro et al. 2001; Nagashima & Yoshii 2004; Ricotti & Gnedin 2005; Marcolini et al. 2006; Valcke, De Rijcke, Dejonghe 2008).

The goal of this paper is to investigate whether the photometric scaling relations traced by dEs and Es persist down to the dSphs ($M_V \gtrsim -14$ mag). We also check for possible environmental influences, other than the obvious density-morphology relation (i.e. the fact that dEs/dSphs are found predominantly in high-density environments). We present new data based on our HST/ACS imaging of dSphs/dEs in the Perseus Cluster and combine these with data of early-type galaxies in the Antlia, Fornax, and Virgo Clusters and the Local Group (see section 2). The resulting photometric scaling laws are presented in section 3. We discuss the results in section 4.

2 PHOTOMETRIC DATA

2.1 Perseus Cluster data

The Perseus Cluster (Abell 426) is one of the richest nearby galaxy clusters, with a redshift $v = 5366$ km s^{-1} (Struble & Rood 1999), and at a distance $D = 72$ Mpc (as given by NED). Due to its low Galactic latitude ($b \approx -13°$) it has not been studied in as much detail as other nearby clusters such as Fornax, Virgo and Coma. We have obtained high resolution *Hubble Space Telescope (HST)* Advanced Camera for Surveys (ACS) WFC imaging in the F555W and F814W bands of five fields in the Perseus Cluster core, in the immediate vicinity of NGC1275 and NGC1272, the cluster's brightest members, obtained in 2005 (program GO 10201). The scale of the images is $0.05''$ pixel^{-1}, with a field of view of $202'' \times 202''$, providing a total survey area of ~ 57 arcmin^2. The positions on the sky of these five pointings are presented in Fig. 1. Exposure times were 2368 and 2260 seconds for the F555W and F814W bands, respectively. The fields were chosen to cover the most likely cluster dSphs and dEs identified from ground-based imagery by Conselice, Gallagher, Wyse (2003). For some of these, there is spectroscopic confirmation of their cluster membership (Penny & Conselice 2008). For the others, we use morphological criteria to decide cluster membership. The CAS system for quantifying compactness, asymmetry, and clumpiness/smoothness (Conselice 2003b) proves very useful to reject e.g. background spiral galaxies based on a smoothness criterion and background bright ellipticals based on a compactness criterion (see Penny et al. (2008)). The Perseus dataset straddles the dE-dSph transition at $M_V \sim -14$ mag and is therefore essential to the discussion that follows.

A detailed account of our photometric analysis of the HST/ACS images of Perseus dSphs and of the properties of the individual galaxies will be reported elsewhere (Penny, Conselice, De Rijcke, Held, in prep.).

2.2 Data from the literature

The photometric data, including resolved photometry for surface brightness profiles, of the Local Group dSphs that are identified as Milky Way satellites are collected from Grebel, Gallagher, Harbeck (2003) and Irwin & Hatzidimitriou (1995), adopting the distances listed in Grebel, Gallagher, Harbeck (2003). Data of the M31 dSph satellites is taken from Peletier (1993), Caldwell (1999), Grebel, Gallagher, Harbeck (2003), McConnachie & Irwin (2006), McConnachie, Arimoto, Irwin (2007), and Zucker et al. (2007). Data of three Local Group dSphs that are not linked to a giant host galaxy, the Tucana dSph, DDO210, and KKR25, come from Saviane, Held, Piotto (1996), Grebel, Gallagher, Harbeck (2003), and McConnachie & Irwin (2006). De Rijcke et al. (2005) (D05) and Mieske et al. (2007) provide photometric data on the early-type dwarf galaxy population of the Fornax cluster. Half of the D05 sample consists of dEs from the NGC5044 and NGC5989 groups. The data of the dSphs and dEs in the Antlia cluster are taken from Smith Castelli et al. (2008). Data data for the giant elliptical and for Coma dEs is taken from Graham & Guzmán (2003) (GG03).

This sample of early-type galaxies comprises dwarf spheroidals, with -14 mag $\lesssim$ M_V $\lesssim -8$ mag, dwarf ellipticals, with -19 mag $\lesssim$ M_V $\lesssim -14$ mag, and bright ellipticals, with $M_V \lesssim -19$ mag. We plot the positions of the sample galaxies in diagrams of V-band absolute magnitude vs. *(i)* half-light radius R_e (in kpc), vs. *(ii)* the Sérsic exponent n of the best fitting Sérsic profile, vs. *(iii)* the central V-band surface brightness of the best fitting Sérsic profile, and vs. *(iv)* V$-$I colour. These diagrams are shown in Fig. 2. The datasets are plotted using different symbols that are explained within each panel of the figure. The presence of a

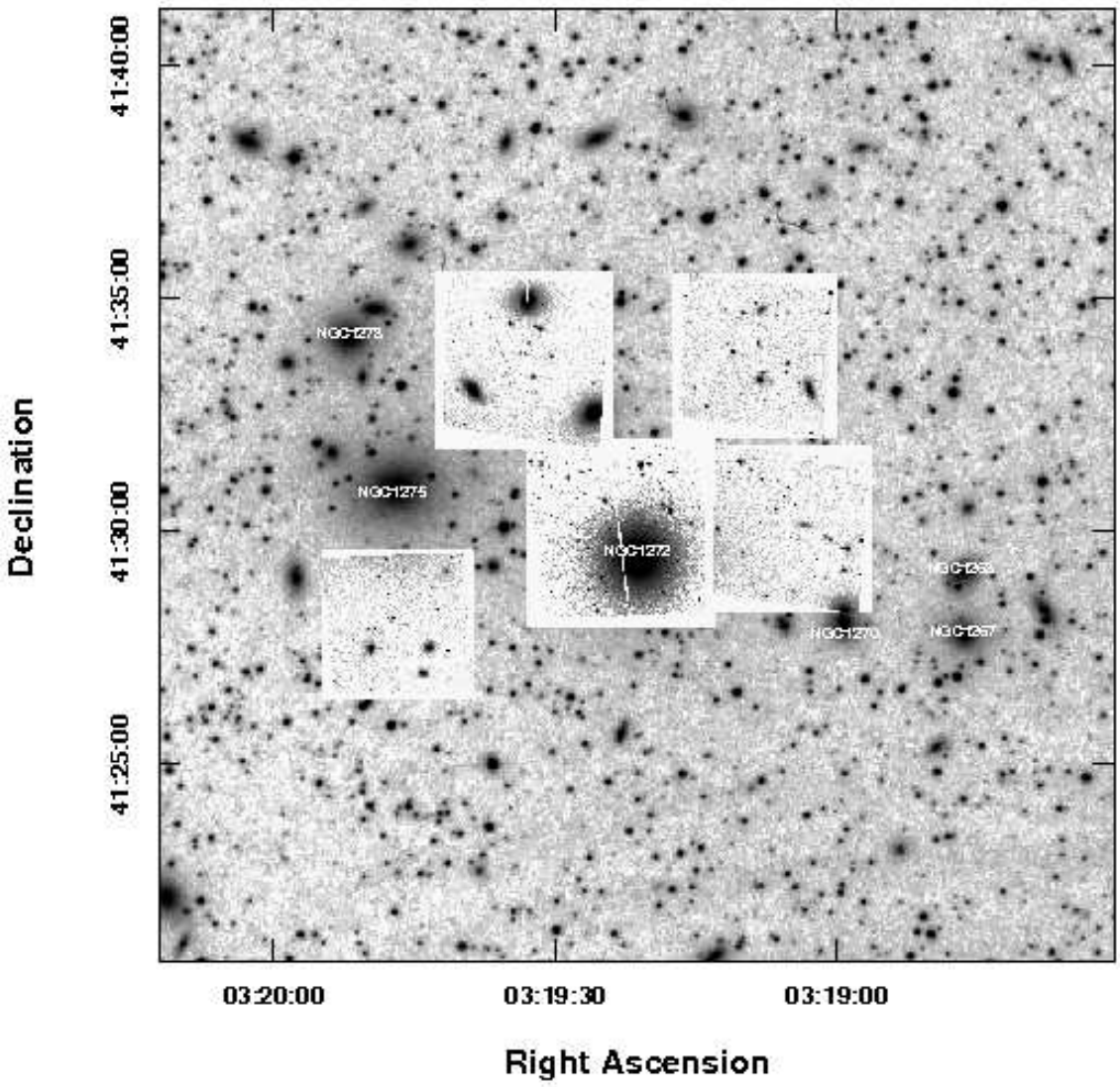

Figure 1. Position on the sky of our five HST/ACS pointings near the core of the Perseus cluster. The HST/ACS fields are overplotted onto a DSS image of the cluster. The NGC-numbers of the most prominent cluster members are indicated in the figure.

dataset in a given panel depends solely on the availability of the required data.

3 PHOTOMETRIC SCALING RELATIONS

3.1 Method

For our Perseus dSphs/dEs, we measure the profiles of surface-brightness, position angle, and ellipticity as a function of the geometric mean of major and minor axis distance, denoted by a and b respectively, using our own software. Basically, the code fits an ellipse through a set of positions where a given surface brightness level is reached. Residual cosmics, background galaxies, and foreground stars are masked and not used in the fit. The shape of an isophote, relative to the best fitting ellipse, is quantified by expanding the surface brightness variation along this ellipse in a fourth order Fourier series with coefficients S_4, S_3, C_4, and C_3:

$$I(a,\theta) = I(a)\,[1 + C_3(a)\cos(3\theta) + C_4(a)\cos(4\theta) + S_3(a)\sin(3\theta) + S_4(a)\sin(4\theta)] \quad (1)$$

Here, $I(a)$ is the mean surface brightness of an isophote with semi-major axis a, and the angle θ is measured from the major axis. Apparent ABMAG magnitudes in the F555W and F814W bands are calculated using the zero-points given by Sirianni et al. (2005). These magnitudes are corrected for interstellar reddening adopting the color excess E(B−V)= 0.171 mag (Schlegel, Finkbeiner, Davis 1998) and using the prescriptions given in Sirianni et al. (2005). These reddening-corrected magnitudes are finally converted into Johnson V and I band magnitudes using the transformations of Sirianni et al. (2005).

The smooth representation of a galaxy's surface-brightness profile, $I(a,\theta)$, is then subtracted from the original image. We have checked that the result is indeed a pure noise image, free of residuals. $I(a,\theta)$ is integrated over circular apertures out to the last isophote we could reliably measure (which is at $\mu_{\rm ABMAG} \approx 27$ mag arcsec^{-2} in both the F555W and F814W images) to derive model independent structural parameters, such as the total apparent mag-

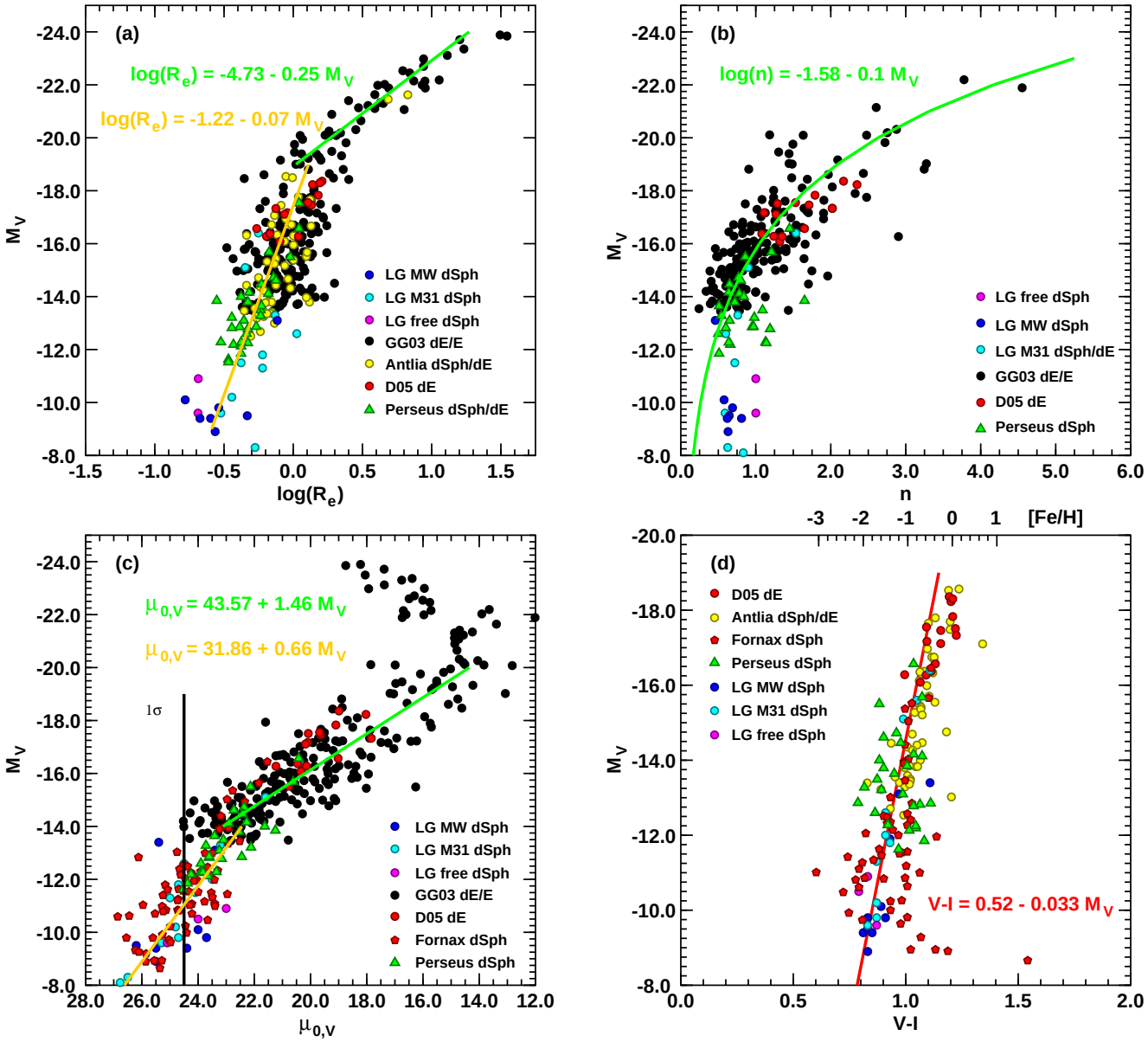

Figure 2. Photometric scaling relations of dwarf spheroidal, dwarf elliptical, and elliptical galaxies. **(a)** Half-light radius, $R_{\rm e}$ (kpc), versus absolute V-band magnitude, $\rm M_V$. The green line traces the relation $\log(R_{\rm e}) = -4.73 - 0.25 \times \rm M_V$ of the bright ellipticals whereas the orange line indicates the relation $\log(R_{\rm e}) = -1.22 - 0.07 \times \rm M_V$ of the dEs and dSphs. **(b)** The Sérsic parameter n versus absolute V-band magnitude. The green curve traces the $\log(n) \propto 0.1 \times \rm M_V$ relation of Graham & Guzmán (2003). **(c)** Central surface brightness $\mu_{0,V}$ (mag arcsec^{-2}), derived by fitting a Sérsic law to the observed galaxies' surface brightness profiles, versus absolute V-band magnitude. The green curve traces the relation $\mu_{0,V} \propto 1.46 \times \rm M_V$ of the dwarf and giant ellipticals; the orange curve is the $\mu_{0,V} \propto 0.66 \times \rm M_V$ relation of the dwarf spheroidals. **(d)** V−I colour versus absolute V-band magnitude (the top x-axis is labeled in metallicity, quantified by [Fe/H], using an empirical relation between V−I and [Fe/H] (Couture, Harris, Allwright (1990); Kundu & Whitmore (1998)). The red line traces the linear fit to the Fornax cluster $\rm M_V$ vs. V−I relation by Mieske et al. (2007). The photometric data of the Local Group dSphs (LG MW dSph for the Milky Way satellites; LG M31 dSph/dE for the M31 satellites; LG free dSph for the dSphs that are not linked to a giant host galaxy) come from Peletier (1993), Irwin & Hatzidimitriou (1995), Saviane, Held, Piotto (1996), Caldwell (1999), Grebel, Gallagher, Harbeck (2003), McConnachie & Irwin (2006), McConnachie, Arimoto, Irwin (2007), Zucker et al. (2007). The other data sets are from Graham & Guzmán (2003) (GG03 dE/E), De Rijcke et al. (2005) (D05 dE), Mieske et al. (2007) (Fornax dSph), Smith Castelli et al. (2008) (Antlia dSph/dE) and this work (Perseus dSph).

nitude and the half-light radius in each band. For such deep images of galaxies with a roughly exponentially declining surface brightness profile, this truncation results in an insignificant uncertainty on the total luminosity, of the order of a few per cent (see also De Rijcke et al. (2005)). V−I colors are measured using the V and I-band flux inside the I-band half-light radius. We fit a Sérsic profile, given by

$$\mu_V(r_p) = \mu_{0,V} + 1.0857 \left(\frac{r_p}{r_0}\right)^{1/n}, \qquad (2)$$

to the V-band surface brightness profiles of the program galaxies, expressed in mag arcsec^{-2}. Here, the equivalent radius $r_p = \sqrt{ab}$ is the geometric mean of the isophotes' semi-major axes a and semi-minor axes b, $\mu_{0,V}$ is the central V-band surface brightness, in mag arcsec^{-2}, r_0 is a scale-length, in arcseconds, and the exponent n is a shape parameter with $n = 1$ giving an exponentially declining profile and $n = 4$ corresponding to the de Vaucouleurs-profile typical of giant ellipticals.

For the Antlia cluster, we adopt a distance of 35.1 Mpc, as advocated by Smith Castelli et al. (2008). This distance estimate is based on surface-brightness fluctuations (SBF) distances to two giant Es in this cluster. As in D05, we place the Fornax cluster at a distance of 19.7 Mpc, the NGC 5044 group at 35.1 Mpc, the NGC 5898 group at 30.3 Mpc, and the NGC 3258 group at 40.7 Mpc, all in good agreement with SBF distances (Tonry, Dressler, Blakeslee 2001; Jerjen 2003). For the GG03 data set, only B-band photometry is available. We convert B-band magnitudes into V-band magnitudes using a B−V color-magnitude relation constructed from the $M_V - (V-I) - [Fe/H]$ relation (see section 3.5) in combination with SSP models for 10 Gyr old stellar populations (Vazdekis et al. 1996). This relation interpolates between B−V ≈ 0.7 mag at $M_B = -8$ mag and B−V ≈ 1.0 mag at $M_B = -22$ mag. As we show below, our conclusions do not depend on this slight color correction applied to the GG03 dataset. There are no systematic deviations of the color corrected GG03 dataset with respect to other datasets with which it overlaps in luminosity. Applying a constant mean color correction $\langle B - V \rangle = 0.8$ mag (van Zee, Barton, Skillman 2004) yields essentially the same results.

For the Local Group dSphs for which no Sérsic parameters can be found in the literature, we fit Sérsic profiles, with an added constant background density of stars, to the star counts of the dSphs presented in Irwin & Hatzidimitriou (1995).

We now place these early-type galaxies in diagrams correlating the V-band absolute magnitude M_V, the Sérsic exponent n, the extrapolated central surface brightness $\mu_{0,V}$, and the V−I colour. The goal is to investigate the behaviour of the relations between these structural parameters as a function of luminosity in the range $-24\,\mathrm{mag} < M_V < -8$ mag and of environment, using galaxies from the Local Group, the NGC5044 and NGC5898 groups, and the Antlia, Fornax, Perseus, and Coma clusters.

3.2 Luminosity vs. half-light radius

We plot V-band absolute magnitude against half-light radius, denoted by R_e, in panel **(a)** of Fig. 2. Es and gEs follow a trend of increasing half-light radius with increasing luminosity, which can be quantified as

$$\log(R_e) = (-4.73 \pm 0.47) - (0.25 \pm 0.02) \times M_V \qquad (3)$$

between $M_V \sim -19$ mag and $M_V \sim -24$ mag (green line in panel **(a)** of Fig. 2). In the range $-19\,\mathrm{mag} \lesssim M_V \lesssim -14$ mag, on the other hand, the half-light radius of dEs increases much more slowly as a function of luminosity, with

$$\log(R_e) = (0.92 \pm 0.14) - (0.05 \pm 0.01) \times M_V \qquad (4)$$

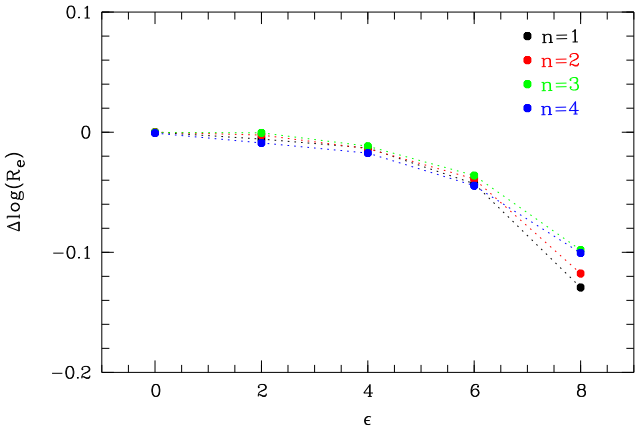

Figure 3. Deviation of the logarithm of the half-light radius measured using circular apertures from the half-light radius defined as the geometric mean of the semi-major axis a and semi-minor axis b of the elliptical isophote that encloses half the light as a function of flattening $\epsilon = 10(1-b/a)$. This exercise was performed for synthetic surface brightness profiles with Sérsic $n = 1$, 2, 3, and 4. The maximum deviation is not larger than $\Delta \log(R_e) \approx 0.15$.

(see also Graham & Guzmán (2003); De Rijcke et al. (2005); Smith Castelli et al. (2008); Graham & Worley (2008)). In the very low-luminosity dSph regime, radius again appears to increase slightly more rapidly with luminosity as

$$\log(R_e) = (-1.40 \pm 0.16) - (0.09 \pm 0.01) \times M_V, \qquad (5)$$

between $M_V \sim -8$ mag and $M_V \sim -14$ mag. This trend appears to continue for even fainter Milky Way satellites (Martin, de Jong, Rix 2008). The very gentle slope change around $M_V \sim -14$ mag seems to be caused mostly by the GG03 data set. All other datasets rather suggest that half-light radius behaves as a power-law as a function of luminosity in the regime $M_V \gtrsim -19$ mag. A fit to the data of the dwarf galaxies fainter than $M_V = -19$ mag from the D05, Antlia, Perseus and Local Group datasets gives

$$\log(R_e) = (-1.22 \pm 0.11) - (0.07 \pm 0.01) \times M_V \qquad (6)$$

(orange line in panel **(a)** of Fig. 2). The gentle curvature of the $M_V - R_e$ relation around $M_V \sim -19$ mag was shown by Graham & Guzmán (2003) to be a consequence of the power-law dependence of the Sérsic parameters on galaxy luminosity.

One small caveat, however: the half-light radius can be measured in a number of different ways which do not necessarily yield the same result for a given galaxy. One can, for instance, use the geometric mean of the semi-major axis and semi-minor axis of the elliptical isophote that encloses half the light as a measure for R_e. Or one can fit a Sérsic law to the surface brightness profile, evaluated as a function of equivalent radius, and adopt the half-light radius of this model profile, as in Graham & Guzmán (2003). Or one can construct the growth curve model-independently by integrating the observed surface brightness over circular apertures and thus derive a half-light radius, as in De Rijcke et al. (2005). For spherically symmetric galaxies, these different approaches obviously yield the same result. For very flattened galaxies, they may differ. If the early-

type galaxy population shows a trend of mean flattening with luminosity (see e.g. Bender et al. (1989)), this might introduce a spurious trend of half-light radius with luminosity.

In order to check how large this systematic effect can be, we create synthetic galaxy images using flattened Sérsic profiles with different flattenings $\epsilon = 10(1 - b/a)$ and Sérsic exponents n. The half-light radius is then measured as the geometric mean of the semi-major axis and semi-minor axis of the elliptical isophote that encloses half the light and by integrating over circular isophotes. The difference between the two approaches is plotted in Fig. 3 as a function of flattening ϵ and Sérsic n. The maximum deviation is obtained for small n and strong flattening and is not larger than $\Delta \log(\mathrm{R_e}) \approx 0.15$. This is smaller than the scatter on the observed scaling relations. We therefore do not expect to see any significant systematic trend of half-light radius with flattening as a result of the particular way it was measured.

Although the data show considerable scatter, especially in the dwarf regime, it is striking that galaxies from a wide range of environments trace a continuous M_V vs. $\mathrm{R_e}$ relation over a range of 6 orders of magnitude in luminosity.

3.3 Luminosity vs. Sérsic n

It is well known that early-type galaxies brighter than $\mathrm{M}_V \sim -14$ mag trace a single M_V vs. n relation. This relation is quantified as $\log(n) = -1.4 - 0.1 \times \mathrm{M}_B$ by Jerjen & Binggeli (1997), as $\log(n) = -1.88 - 0.12 \times \mathrm{M}_{\mathrm{F606W}}$ by Graham & Guzmán (2003), and as $\log(n) = -1.52 - 0.11 \times \mathrm{M}_B$ by Graham & Worley (2008). These authors fit Sérsic profiles to the observed surface brightness profiles, evaluated as function of equivalent radius. However, it is also possible to fit the growth curve, constructed by integrating a galaxy image over circular apertures, with the growth curve of the Sérsic profile. This approach is advocated by Prugniel & Simien (1997). The latter method of determining the Sérsic exponent n assigns a large weight to the outer data points and has the obvious advantage of yielding a Sérsic model with the same total luminosity as the observed galaxy. However, the model's surface brightness profile does not necessarily provide an acceptable fit to that of the observed galaxy. The former method, on the other hand, assigns a large weight to the inner data points. This method has the benefits that clearly non-Sérsic components (such as a nuclear star cluster of a stellar halo) can be omitted from the fit and that the model provides a good fit to the observed surface brightness profile (at least within some specified radial range). It does not, however, necessarily provide a good approximation of the galaxy's growth curve.

As an example, we apply both methods to the Sculptor dSph, with star count data taken Irwin & Hatzidimitriou (1995), and to our new HST/ACS photometry of CGW45, a Perseus cluster dE, taken from the sample of Conselice, Gallagher, Wyse (2003). The observed surface brightness profile of CGW45, $\mu(r)$, is converted into a "star counts" profile in arbitrary units, $n(r)$ using

$$n(r) = 10^{(20-\mu(r))/2.5}. \quad (7)$$

Sculptor is an example of a galaxy whose surface brightness profile deviates from a Sérsic law at large radii; CGW45, a nucleated dE, on the other hand, deviates from a Sérsic profile at small radii. The differences between the two methods for obtaining n are illustrated in Fig. 4. A fit to the stellar density profile of Sculptor yields $n \approx 0.7$; a fit to the growth curve results in $n \approx 1.0$. The former method yields a very good approximation to both the growth curve and the density profile within the inner 30 arcmin but fails at larger radii. The latter method gives a superior fit to the growth curve outside 30 arcmin but fails to provide an acceptable fit to the density profile. In the case of CGW45, both methods give $n \approx 1.4$. The central nucleus prevents both methods from yielding a good fit to the growth curve within the inner $0.2''$. Omitting the central $0.2''$ results in a very good Sérsic fit to the density profile.

Choosing between these two methods is clearly a matter of taste. Here, as in Graham & Guzmán (2003), we wish n to reflect the shape of the surface brightness profile of the bulk of the galaxy and, therefore, opt to fit a Sérsic profile to the surface brightness profile evaluated as a function of equivalent radius.

It is obvious from panel **(b)** of Fig. 2 that for galaxies fainter than $\mathrm{M}_V \sim -14$ mag the relation between luminosity and n appears to break down. The dwarf spheroidals for which the Sérsic exponent n is available, i.e. the Local Group dSphs, for some of which we have measured n using published star counts (Irwin & Hatzidimitriou 1995), and our new Perseus cluster dSphs, all lie in the range $n \approx 0.5$ to 1.0, essentially independent of galaxy luminosity. This n is significantly larger than that predicted by the scaling relations mentioned before (green curve). It is, therefore, clear that in the dSph regime, the power-law behaviour of the $\mathrm{M}_V - n$ relation breaks down.

From Fig. 5, it is clear that a Sérsic profile with $0.5 \lesssim n \lesssim 1$ is almost indistinguishable from a King model with a concentration $c = r_{\mathrm{tidal}}/r_{\mathrm{core}}$ in the range 3 to 10, which is typical for dSphs. In this figure, we plot the radial profile of projected stellar density of the Sculptor dSph (black data points), taken from Irwin & Hatzidimitriou (1995), overplotted with the best fitting Sérsic profile (red line) and King profile (green line). The Sérsic profile has a shape parameter $n = 0.7$; the concentration of the King profile is $c = r_{\mathrm{tidal}}/r_{\mathrm{core}} = 4.25$. Both 3-parameter laws give a very good representation of the data, taking into account a background density of 1.13 arcmin^{-2}. Thus, the breakdown of the power-law dependence of n on luminosity in the dSph regime might have been foreseen based on the already known fact that $c \gtrsim 3$ for dSphs.

Sharina et al. (2008) fit the surface brightness profiles of a sample of Local Volume dSphs, dIrrs, and brighter late-type galaxies with exponentials and investigate the resulting relation between luminosity and exponential scale-length, denoted by h. They note that the luminosity-h relation becomes almost flat in the dSph regime. This is a direct consequence of the $\mathrm{M}_V - \mathrm{R_e}$ and $\mathrm{M}_V - n$ relations presented here. We generate synthetic Sérsic surface brightness profiles using the latter relations. We fit these synthetic surface brightness profiles with exponentials and thus constructed a $\mathrm{M}_V - h$ relation. This relation is in excellent agreement with the one found observationally by Sharina et al. (2008). Between $\mathrm{M}_V = -10$ mag and $\mathrm{M}_V = -14$ mag, the exponential scale-length increases only from 0.25 kpc to 0.5 kpc. This $\mathrm{M}_V - h$ relation is much shallower than the $\mathrm{M}_V - \mathrm{R_e}$ re-

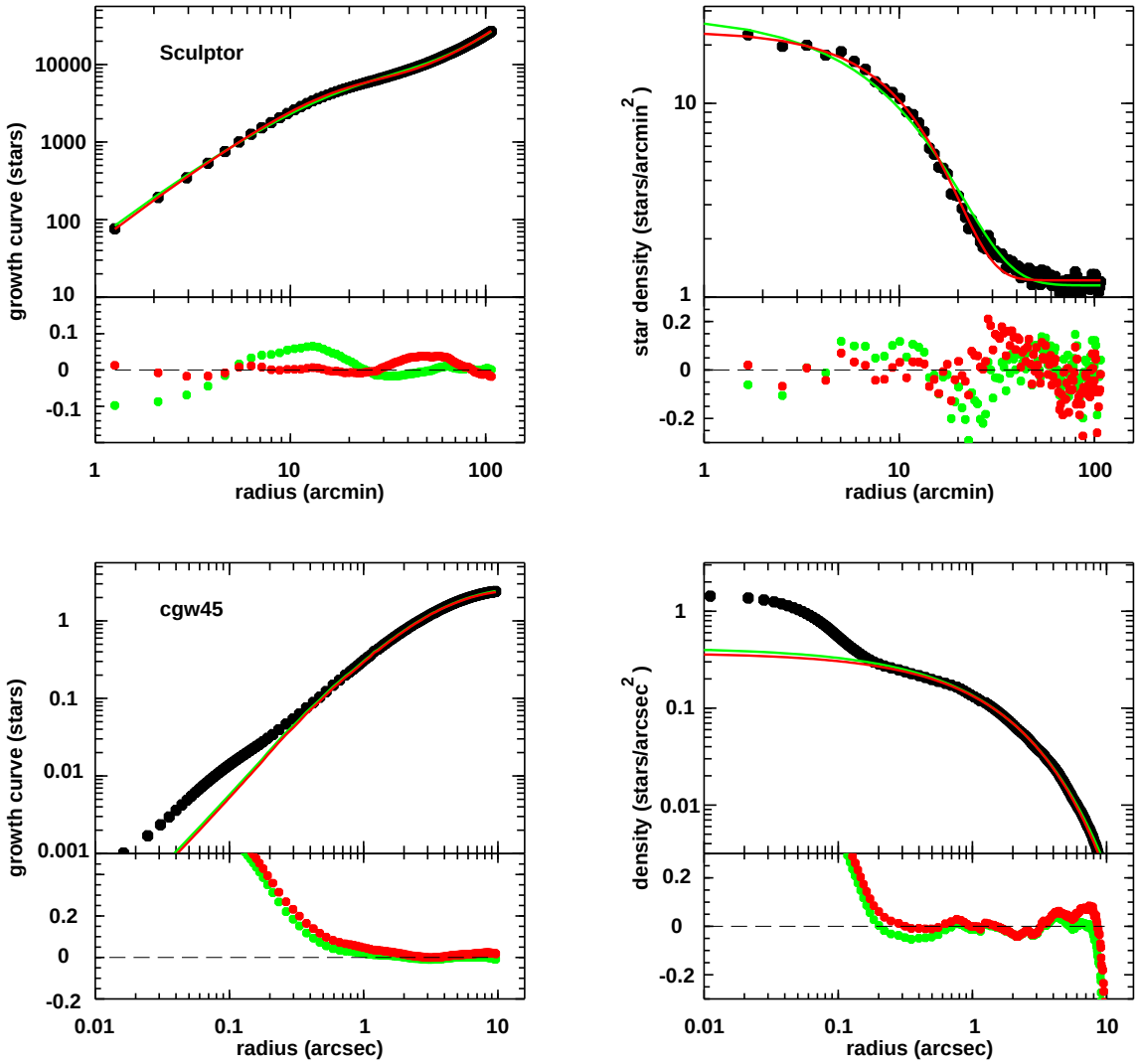

Figure 4. The growth curve (left panels) and the radial profile of the projected stellar density (right panels) of the Sculptor dSph (top row), taken from Irwin & Hatzidimitriou (1995), and the Perseus cluster dSph CGW45 (bottom row), taken from the Conselice, Gallagher, Wyse (2003) sample . The stellar density of CGW45 is in arbitrary units. The black dots represent the data; the red line is a Sérsic profile fitted to the projected stellar density profile; the green line is a Sérsic profile fitted to the growth curve. Under each panel, the relative residuals are plotted in the same colours. Sculptor is an example of a galaxy whose surface brightness profile deviates from a Sérsic profile at large radii; CGW45 is a nucleated dwarf elliptical galaxy and deviates from a Sérsic profile at small radii.

lation because of the increase of n with M_V, which makes brighter galaxies more centrally concentrated than fainter ones.

3.4 Luminosity vs. central surface brightness

The $M_V - \mu_{0,V}$ diagram is presented in panel **(c)** of Fig. 2. The vertical black line marks the 1σ background noise level of our HST/ACS images, translated into a V-band surface brightness. We can only derive reliable surface photometry for galaxies with a central surface brightness above roughly this background limit, corresponding to $\mu_{BG,V} = 24.5$ mag arcsec^{-2}. For galaxies brighter than $M_V \sim -14$ mag, the central surface brightness, estimated by extrapolating the best fitting Sérsic profile to zero radius, varies as a power of the luminosity. Only the very brightest cored gEs deviate from this power law. This underlying unity between Es and dEs was not initially appreciated since it is not reflected in the luminosity vs. mean and effective surface brightness diagrams (Graham & Guzmán 2003). Using the Sérsic parameters as fundamental morphological parameters, the assumed structural dichotomy between Es and dEs has disappeared and the idea that similar physical processes have governed the evolution of *all* spheroidal galaxies was put forward.

However, for galaxies fainter than $M_V \sim -14$ mag, the slope of the $\mu_{0,V} - M_V$ relation changes significantly. This is a direct consequence of the near constancy of n in this luminosity regime, with $n \approx 0.8$ (panel **(b)** of Fig. 2), and the observed $M_V - R_e$ relation (panel **(a)** of Fig. 2). At constant n, the latter translates into a $M_V - r_0$ relation, with r_0 the scale-radius of the Sérsic profile, that is completely

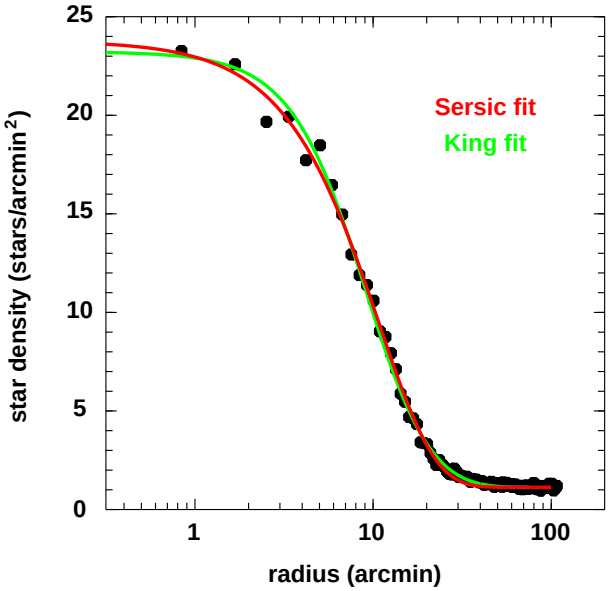

Figure 5. The radial profile of the projected stellar density overplotted (black dots) with the best fitting Sérsic profile (red line) and King profile (green line). The Sérsic profile has a shape parameter $n = 0.7$; the concentration of the King profile is $c = r_{\rm tidal}/r_{\rm core} = 4.25$. A constant background of 1.13 arcmin^{-2} was added to the two profiles.

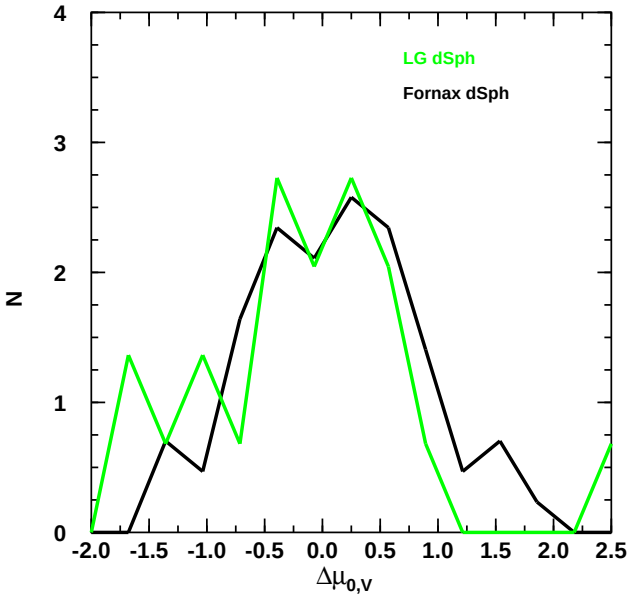

Figure 6. Distribution of the surface brightness deviation of the Local Group dSphs (green curve) and Fornax dSphs (black curve) from the mean relation $\mu_{0,V} = (31.86\pm0.43)+(0.66\pm0.04)\times {\rm M}_V$, denoted by $\Delta\mu_{0,V}$. Both distributions have the same normalization. Only galaxies fainter than ${\rm M}_V = -14$ mag have been selected for this exercise. The Fornax cluster clearly contains a low-surface brightness population that is absent from the other datasets. The offset between the means of these distributions is about 0.2 mag arcsec^{-2}.

similar to the ${\rm M}_V - {\rm R}_{\rm e}$ relation. Given $n = 0.8$ and this ${\rm M}_V - {\rm r}_0$ relation, the central surface brightness should follow the relation

$$\mu_{0,V} = 29.68 + 0.46 \times {\rm M}_V \quad [{\rm dSph}]. \tag{8}$$

A linear fit to the dSphs from the Local Group, the Perseus Cluster, and the Fornax cluster yields

$$\mu_{0,V} = (31.86 \pm 0.43) + (0.66 \pm 0.04) \times {\rm M}_V \quad [{\rm dSph}], \tag{9}$$

plotted as a orange line in Fig. 2. This differs signifcantly from the relation

$$\mu_{0,V} = (43.57 \pm 0.96) + (1.46 \pm 0.06) \times {\rm M}_V \quad [{\rm dE + E}] \tag{10}$$

fitted to the Graham & Guzmán (2003) dEs and Es (green line). It is important to note that the slope change around ${\rm M}_V = -14$ mag is immediately evident from the data sets for the dwarf populations of the Fornax cluster and the Perseus cluster, which cover the transition region in the ${\rm M}_V - \mu_{0,V}$ diagram. Hence, within the same environment, dSphs (${\rm M}_V \gtrsim -14$ mag) and dEs/Es (${\rm M}_V \lesssim -14$ mag) follow a ${\rm M}_V - \mu_{0,V}$ relation with a slope that varies as a function of luminosity. Early-type galaxies from different environments (the Local Group, Fornax, Coma, Perseus, ...) all fall on the same ${\rm M}_V - \mu_{0,V}$ relation. This shows that the slope of this relation is a strong function of galaxy luminosity but not of environment.

As Mieske et al. (2007) note, their sample includes a population of dSphs that have much fainter central surface brightnesses than those of the Local Group. Our HST/ACS imaging, unfortunately, does not go deep enough to detect such a population in the Perseus cluster. In order to quantify the effect of this population on the global scaling relation, we measure the surface brightness deviation of the Fornax dSphs and of the Local Group and Perseus cluster dSphs from the straight-line relation given by eq. (9). This deviation of surface brightness from the mean relation is denoted by $\Delta\mu_{0,V}$. Only galaxies fainter than ${\rm M}_V = -14$ mag have been selected for this exercise. For the Fornax dSphs, the distribution of this deviation shows a pronounced tail towards large, positive $\Delta\mu_{0,V}$ (see Fig. 6). This is the signature of the low-surface brightness population. This population is clearly absent from the Local Group and Perseus dSph datasets. However, the mean $\Delta\mu_{0,V}$ of the Fornax dSph population differs less than 0.2 mag arcsec^{-2} from that of the Perseus and Local Group populations.

Interestingly, dSphs seem to trace the same ${\rm M}_V - \mu_{0,V}$ relation as the dIrrs within the local 10 Mpc volume, which was quantified as

$$\mu_{0,V} = 29.29 + 0.52 \times {\rm M}_V \quad [{\rm dIrr}] \tag{11}$$

by Sharina et al. (2008). If star formation was somehow switched off in dIrrs that are initially on this relation, fading of ${\rm M}_V$ and $\mu_{0,V}$ over time by roughly the same amount (in magnitudes) would result in exactly such a population of very low surface brightness dSph-like objects.

So, while Es and dEs seem to follow a linear relation between ${\rm M}_V$ and $\mu_{0,V}$, dSphs deviate significantly from this relation. They have a higher central surface brightness than predicted by the extrapolated relation of dEs and Es, albeit with the existence of a possible cluster population of very low surface brightness dSphs, which, Mieske et al. (2007)

surmise could be a population of tidally heated dwarf galaxies.

3.5 Luminosity vs. V−I colour

The V−I colours of early-type dwarfs of the Perseus cluster, with both V- and I-band magnitudes measured within the I-band half-light radius, are plotted versus V-band absolute magnitude in panel **(d)** of Fig. 2. The same data for Fornax cluster early-type dwarfs have been taken from Mieske et al. (2007) and plotted in the same panel. A linear fit to the Fornax cluster M_V vs. V−I relation is overplotted (full red line). The Perseus dwarfs obviously adhere quite closely to the color-magnitude relation (CMR) defined by the Fornax dwarfs.

In order to investigate the physical nature of the CMR, we convert the Iron abundance [Fe/H], measured by Michielsen et al. (2007) for the D05 sample of cluster and group dEs, into a V−I color using an empirical color-metallicity relation calibrated for old stellar populations, such as globular clusters (Couture, Harris, Allwright 1990; Kundu & Whitmore 1998). This places the D05 dwarfs essentially along the extension of the Mieske et al. (2007) CMR. The same exercise can be done for the Local Group dSphs, with the metallicity taken from the compilation by Grebel, Gallagher, Harbeck (2003), with the same result: they end up following the Mieske et al. (2007) CMR. This already suggests that the V−I CMR of early-type dwarf galaxies is, in fact, a luminosity-metallicity relation. As a further test, we convert the $C-T_1$ colors of the Antlia dSphs/dEs, measured by Smith Castelli et al. (2008), into V−I colors using empirical $(C-T_1)-$[Fe/H] and [Fe/H]$-(V-I)$ relations as an intermediate step. This places the Antlia dSphs/dEs almost exactly on the extension of the CMR of the Fornax dSphs.

Thus, it appears that the observed V−I CMR of early type galaxies, from dwarfs to giants, is a luminosity-metallicity relation of galaxies that have stopped forming stars sufficiently long ago for there being almost no age information left (see also Smith Castelli et al. (2008) and references therein).

4 DISCUSSION AND CONCLUSIONS

We have collected photometric data of dSphs/dEs from different galaxy groups and clusters. Analogous to Goto et al. (2003), we quantify the galaxy densities of the different environments we are studying as the projected density of galaxies brighter than $M_B = -19$ mag within the radius d_5 that contains five such galaxies, or:

$$\Sigma_5 = \frac{5}{\pi d_5^2}\,\mathrm{galaxies\,Mpc^{-2}}. \qquad (12)$$

The $\log(\Sigma_5)$-values of the different environments from which we compiled the dataset are listed in Table 1.

The Local Group and the NGC5989 group constitute the sparsest environments covered by the dataset (the NGC5989 group consists of two bright ellipticals, NGC5903 and NGC5898, and a few tens of much fainter galaxies; Gourgoulhon, Chamaraux, Fouqué (1992) list only three group members brighter than $M_B \approx -18$ mag). The Fornax cluster and the NGC5044 group have comparable, intermediate bright galaxy densities. The Coma, Perseus, and Antlia clusters have the most extreme central bright galaxy densities. Obviously, the dataset contains early-type galaxies from a wide variety of environments.

Table 1. Central bright-galaxy density, measured by $\log(\Sigma_5)$ (see eq. (12)), of the different environments from which the dataset was composed.

group/cluster	$\log(\Sigma_5)$
Local Group	-0.9
NGC5898 group	-0.7
Fornax cluster	0.5
NGC5044 group	0.7
Antlia cluster	1.5
Perseus cluster	1.8
Coma cluster	2.0

There is considerable uniformity in the photometric properties of early-type galaxies, from dwarfs to giants. Photometric parameters quantifying the structure and stellar populations of early-type galaxies, such as the half-light radius, R_e the central surface brightness $\mu_{0,V}$, the Sérsic exponent n, and V−I color all correlate with galaxy luminosity over a range of more than 6 orders of magnitude in luminosity. The scaling relations involving the Sérsic parameters, contrary to previous claims, do not keep a constant slope over the whole luminosity range. The Sérsic exponent n varies with luminosity L as $n \propto L^{0.25-0.3}$ for galaxies brighter than $M_V \approx -14$ mag but scatters around a constant value within the range $n \approx 0.5-1.0$ for fainter dSphs. This is in agreement with the fact that the surface brightness profiles of dSphs can be well approximated by King profiles with a concentration in the range $c \approx 3-10$. Central surface brightness increases with luminosity until the formation of the very brightest, cored ellipticals. **The cores in the most luminous ellipticals are thought to result from the partial evacuation of the nuclear region by coalescing black holes (see GG03 and references therein).** At $M_V \approx -14$ mag, the slope of the $M_V - \mu_{0,V}$ changes abruptly. We have shown that the M_V vs. V−I is essentially a metallicity-luminosity relation of old stellar populations, keeping the same slope over the whole luminosity range investigated here.

Clearly, the absolute magnitude $M_V \approx -14$ mag is not just an arbitrary divide between dSphs and dEs. The rather abrupt changes in the slopes of some of the photometric scaling relations suggest that below and above this luminosity, different physical processes dominate the evolution of early type galaxies. The near-independence of these scaling relations with respect to environment and the physical differences between dSphs and dEs will be investigated theoretically using N-body/SPH-models in another paper in this series (De Rijcke, Valcke, Conselice, Penny, Held, in prep.). In a sense, the divide between dEs and Es, which has historically been placed at $M_V \approx -19$ mag seems more arbitrary since the behaviour of the basic parameters de-

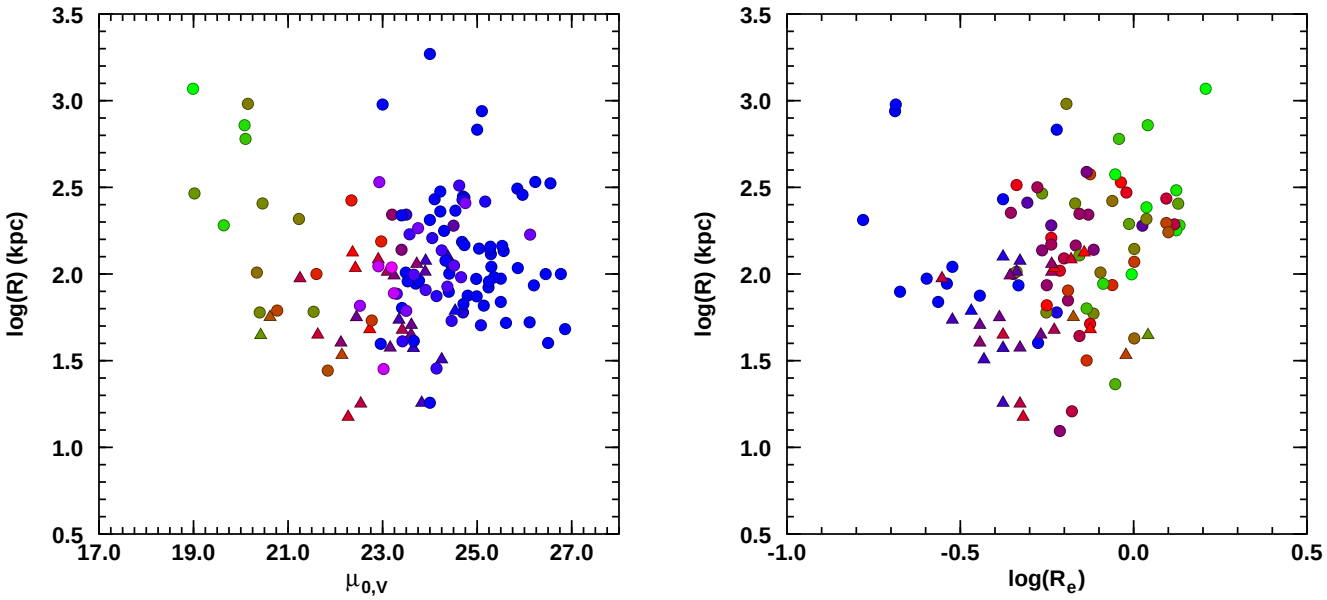

Figure 7. Central surface brightness, $\mu_{0,V}$ (left panel), and half-light radius, R_e (right panel), as a function of projected distance (in kpc), R, to the nearest bright galaxy (with $M_V < -20$ mag). The triangle data points are the Perseus dSphs. In the left panel, the necessary data are available for the dSphs/dEs of the Local Group, the Perseus dSphs, and the Fornax cluster dSphs/dEs from D05 and Mieske et al. (2007). In the right panel, we use data from the dSphs/dEs of the Local Group, the Perseus dSphs, the Fornax cluster dEs from D05, and the Antlia dSpsh/dEs from Smith Castelli et al. (2008). The data points are color coded according to their absolute luminosity, from blue ($M_V = -11$ mag) over red ($M_V = -14$ mag) to green ($M_V = -18$ mag). While there is no statistically significant correlation between these structural parameters and distance to the nearest bright galaxy there is a clear correlation with luminosity.

scribing the shapes of the surface brightness profiles as a function of luminosity (i.e. the Sérsic parameters) does not change. A comparison of numerical simulations with observed scaling relations suggests that the luminosity dependence of the Sérsic parameters is due to fact that the effects of supernova feedback become more important as galactic gravitational potential wells become more shallow for lower galaxy masses (Carraro et al. 2001; Nagashima & Yoshii 2004; Valcke, De Rijcke, Dejonghe 2008). This causes dEs to be more diffuse and to have stars orbiting with lower velocities than predicted by the extrapolated relations for Es (Held et al. 1992; Graham & Guzmán 2003; Matković & Guzmán 2005; De Rijcke et al. 2005).

These scaling relations are amazingly insensitive to (local) environment. In Fig. 7, we show the central surface brightness, $\mu_{0,V}$ (left panel), and half-light radius, R_e (right panel), as a function of projected distance (in kpc), R, to the nearest bright galaxy (with $M_V < -20$ mag). The triangle data points are the Perseus dSphs. In the left panel, the necessary data are available for the dSphs/dEs of the Local Group, the Perseus dSphs, and the Fornax cluster dSphs/dEs from D05 and Mieske et al. (2007). In the right panel, we use data from the dSphs/dEs of the Local Group, the Perseus dSphs, the Fornax cluster dEs from D05, and the Antlia dSpsh/dEs from Smith Castelli et al. (2008). The data points are color coded according to their absolute luminosity, from blue ($M_V = -11$ mag) over red ($M_V = -14$ mag) to green ($M_V = -18$ mag). While there is no statistically significant correlation between these structural parameters and distance to the nearest bright galaxy there is a strong correlation with luminosity.

We have also plotted these quantities as a function of distance to the cluster or group center divided by the virial radius R_{200}. Again, no correlation with position becomes apparent. The galaxies with central surface brightness $\mu_{0,V} \approx 23$ mag arcsec^{-2}, where the slope of the $M_V - \mu_{0,V}$ relation changes, have nearest neighbor distances scattering between 20 and 300 kpc. However, they all have luminosities $M_V \approx -14$ mag. From this exercise, we can conclude that the photometric scaling relations presented in Fig. 2 are not a consequence of environmental segregation, with fainter galaxies preferentially located close to a bright galaxy.

Park & Choi (2008) study the structural parameters such as the concentration index, Petrosian radius, velocity dispersion, u−r colour, . . . of a volume-limited sample of 49,571 galaxies extracted from the SDSS. They show that these parameters are almost independent of large-scale density and neighbor separation unless the latter is smaller than about one-tenth of the bright neighbor's virial radius, i.e., of the order of a few tens of kpc (their Figs. 7 and 9). All galaxies presented in the present paper have projected distances between 0.1 and 1 virial radii away from their nearest bright neighbor and, as Park & Choi (2008), we observe no significant relation between nearest-neighbor distance or environment density and structural properties in this regime. This also corroborates the re-

sults of Weinmann et al. (2008) who study a sample of galaxies selected from the SDSS DR4 and find that the structural properties of early-type satellite galaxies are very similar to early-type central galaxies. Hence, the structure of early-type galaxies is not significantly affected by environmental effects.

The most obvious environmental effect appears to be the population of low surface brightness dSphs discovered by Mieske et al. (2007) in the Fornax cluster. Where an environmental influence is clearly discernible, it has only mild effects on the scaling relations. The presence of a low-surface brightness population of Fornax dSphs doesn't affect the global scaling relation appreciably. At a given luminosity, the Fornax dSph population is on average 0.2 mag arcsec^{-2} fainter than the Perseus and Local Group dSph populations. The M31 companions with tidal extensions or distorsions (Ségall et al. 2007; Lewis et al. 2007) are not displaced from the general scaling relations. This may indicate that dSphs intrinsically have high enough M/L to survive unscathed (see Penny et al. (2008)) or that dSphs with too low M/L have been destroyed and only those with high M/L survive to the present day.

ACKNOWLEDGMENTS

SDR wishes to thank Philippe Prugniel and Mina Koleva for their hospitality and for the stimulating discussions while visiting CRAL Lyon Observatory during the course of this work. CJC and SJP acknowledge support from STFC. SDR is a Postdoctoral Fellow of the Fund for Scientific Research - Flanders (Belgium)(F.W.O). SV is a PhD Fellow of the Fund for Scientific Research - Flanders (Belgium)(F.W.O). This research has made use of the NASA/IPAC Extragalactic Database (NED) which is operated by the Jet Propulsion Laboratory, California Institute of Technology, under contract with the National Aeronautics and Space Administration.

REFERENCES

Bender R., Surma P., Döbereiner S., Möllenhoff C., Madejsky R., A&A, 217, 35
Blitz L. & Robishaw T., 2000, ApJ, 541, 675
Buyle P., De Rijcke S., Michielsen D., Baes M., Dejonghe H., 2005, MNRAS, 360, 853
Caldwell N., 1999, AJ, 118, 1230
Carraro G., Chiosi C., Girardi L., Lia C., 2001, MNRAS, 335, 335
Conselice C. J., Gallagher, J. S., III, Wyse R. F. G., 2003, AJ, 125, 66
Conselice, C.J., O'Neil, K., Gallagher, J.S., Wyse, R.F.G. 2003, ApJ, 591, 167
Conselice C. J., 2003, ApJS, 147, 1
Couture J., Harris W. E., Allwright J. W. B., 1990, ApJS, 73, 671
De Rijcke S., Zeilinger W. W., Dejonghe H., Hau G. K. T., 2003, MNRAS, 339, 225
De Rijcke S., Michielsen D., Dejonghe H., Zeilinger W. W., Hau G. K. T., 2005, MNRAS, 360, 853 (D05)
De Rijcke S., Prugniel P., Simien F., Dejonghe H., 2006, MNRAS, 369, 1321
De Rijcke S., Zeilinger W. W., Hau G. K. T., Prugniel P., Dejonghe H., 2007, ApJ, 659, 1172
Goto T., Yamauchi C., Fujita Y., Okamura S., Sekiguchi M., Smail I., Bernardi M., Gomez P. L., 2003, MNRAS, 346, 601
Gourgoulhon E., Chamaraux P., Fouqué P., A&A, 255, 69
Graham A. W. & Guzmán R., 2003, AJ, 126, 1787 (GG03)
Graham A. W. & Worley C. C., 2008, accepted for publication in MNRAS, 2008arXiv0805.3565
Grebel E. K., Gallagher J. S. III, Harbeck D., 2003, AJ, 125, 1926
Held E. V., de Zeeuw T., Mould J., Picard A., 1992, AJ, 103, 851
Irwin M. & Hatzidimitriou D., 1995,
Jerjen H. & Binggeli B., 1997, The Nature of Elliptical Galaxies, 2nd Stromlo Symposium. ASP Conference Series, Vol. 116, 1997, eds. M. Arnaboldi, G. S. Da Costa, and P. Saha (1997), p.239
Jerjen H., 2003, A&A, 398, 63
Johnston K. V., Spergel D. N., Hernquist L., 1995, ApJ, 451, 598
Kleyna J. T., Wilkinson M. I. Evans N. W., Gilmore G., 2005, ApJ, 630, L141
Kundu A. & Whitmore B. C., 1998, AJ, 116, 2841
Lewis G. F., Ibata R. A., Chapman S. C., McConnachie A., Irwin M. J., Tolstoy, E., Tanvir N. R., 2007, MNRAS, 375, 1364
Lisker T., Glatt K., Westera P., Grebel E. K., 2006, AJ, 132, 2432
Łokas E. L., 2002, MNRAS, 333, 697
Marcolini A., Brighenti F., D'Ercole A., 2003, MNRAS, 345, 1329
Marcolini A., D'Ercole A., Brighenti F., Recchi S., 2006, MNRAS, 371, 64
Martin N. F., de Jong T. A., Rix H.-W., 2008, accepted for publication in ApJ, 2008arXiv:0805.2945
Mateo M., Mirabal N., Udalski A., Szymanski M., Kaluzny J., Kubiak M., Krzeminski W., Stanek K. Z., 1996, ApJ, 458, L13
Mateo M. L., 1998, ARA&A, 36, 435
Mateo M., Olszewski E. W., Walker M. G., 2008, ApJ, 675, 201
Matković A. & Guzmán R., 2005, MNRAS, 362, 289
McConnachie A. W. & Irwin M. J., 2006, MNRAS, 365, 1263
McConnachie A. W., Arimoto N., Irwin M., 2007, MNRAS, 379, 379
Michielsen D. Koleva M., Prugniel P., Zeilinger W. W., De Rijcke S., Dejonghe H., Pasquali A., Ferreras I., Debattista V. P., 2007, ApJ, 670, L101
Mieske S., Hilker M., Infante L, Mendes de Oliviera C., 2007, A&A, 463, 503
Nagashima M. & Yoshii Y., 2004, ApJ, 610, 23
Park C. & Choi Y.-Y., 2008, accepted by ApJ, arXiv:0809.2156
Peletier R. F., 1993, A&A, 271, 51
Penny S. J. & Conselice C. J., 2008, MNRAS, 383, 247
Penny S. J., Conselice C. J., De Rijcke S., Held E. V., 2008, submitted to MNRAS
Prugniel P. & Simien F., A&A, 321, 111

Ricotti M. & Gnedin N. Y., 2005, ApJ, 629, 259
Saviane I., Held E. V., Piotto G., 1996, A&A, 315, 40
Schlegel D. J., Finkbeiner D. P., Davis M., 1998, ApJ, 500, 525
Ségall M., Ibata R. A., Irwin M. J., Martin N. F., Chapman S., 2007, MNRAS, 375, 831
Sharina M. E., Karachentsev I. D., Dolphin A. E., Karachentseva V. E., Tully R. B., Karataeva G. M., Makarov D. I., Makarova L. N., Sakai S., Shaya E. J., Nikolaev E. Y., Kuznetsov A. N., 2008, MNRAS, 384, 1544
Sirianni M., Jee M. J., Benítez N., Blakeslee J. P., Martel A. R., Meurer G., Clampin M., De Marchi G., Ford H. C., Gilliland R., Hartig G. F., Illingworth G. D., Mack J., McCann W. J., 2005, PASP, 117, 1049
Smith Castelli A. V., Bassino L. P., Richtler T., Cellone S. A., Aruta C., Infante L., 2008, MNRAS, 386, 2311
Struble M.F., Rood H.J., 1999, ApJS, 125, 36
Tonry J. L., Dressler A., Blakeslee J. P., et al., 2001, ApJ, 546, 681
Valcke S., De Rijcke S., Dejonghe H., 2008, accepted for publication in MNRAS
van Zee L., Barton E. J., Skillman E. D., 2004, AJ, 128, 2797
Vazdekis A., Casuso E., Peletier R. F., Beckman J. E., 1996, ApJS, 106, 307
Weinmann S., M., Kauffmann G., van den Bosch F. C., Pasquali A., McIntosh D., H., Mo H., Yang X., Guo Y., 2008, submitted to MNRAS, 2008arXiv0809.2283
Young L. M., Skillman E. D., Weisz D. R., Dolphin A. E., 2007, ApJ, 659, 331
Zucker D. B., Kniazev A. Y., Martínez-Delgado D., Bell E. F., Rix H.-W., et al., 2007, ApJ, 659, L21

This paper has been typeset from a TEX/ LATEX file prepared by the author.